Tubular Si-infiltrated SiC_f/SiC composites for solar receiver application – Part 2: Thermal performance analysis and prediction

A. Ortona [a], D.H. Yoon [b], T. Fend*, G. Feckler [c] and O. Smirnova [c]

[a]*ICIMSI, SUPSI, Galleria 2, CH-6928 Manno, Switzerland*

[b]*School of Materials Science and Engineering, Yeungnam University, Gyeongsan 712-749, Korea*

[c]*Institute of Solar Research, German Aerospace Center, Linder Höhe, 51147, Köln, Germany*

*corresponding author: Thomas.Fend@dlr.de

Tel. +49 2203 601 2101

ABSTRACT

Tubular Si-infiltrated SiC_f/SiC composites composed of an inner cellular ceramic and an outer dense ceramic matrix composite (CMC) skin have been fabricated by the electrophoretic deposition of matrix phases followed by Si-infiltration for pre-feasibility testing in solar receiver applications. The tubes have been considered to be used as high temperature receiver components for the solar operation of a gas turbine or a combined cycle with temperatures up to 1100°C and typical pressures of more than 6 bars. The cellular structure inside the tube has been introduced for improvement of the heat transfer from the irradiated outer surface of the tube to the working fluid inside. Heat transfer and permeability characteristics of the composite samples have been determined experimentally as effective properties. These properties have been used in numerical models to predict the performance of such kind of components in gas turbine service conditions. It could be demonstrated, that the heat transfer rate in a tube with a porous in-lay could be increased to approximately four times compared to the rate of an empty tube of the same size. The results of the study give reason for further experimental testing in service environments.

1. Introduction

Due to beneficial thermal properties, the use of Si-infiltrated SiC fiber-reinforced SiC (SiC_f/Si/SiC) composites offers great chances for a significant improvement of high temperature components such as heat exchangers, recuperators, solar receivers and many

more. In nearly all of these applications high temperature strength, thermal shock resistance, large thermal conductivities and large specific surfaces for heat transfer are needed [1].

The present study is focused on the application as a tubular high temperature receiver for the solar gas turbine [2]. This component is aimed at being placed in the focus of a *Solar Tower*, a large scale installation to generate electricity from concentrated solar radiation, where it is operated at typical temperatures of 1200-1300°C [3].

The principle concept of a solar driven gas turbine or a solar driven combined cycle has been already proposed earlier [4, 5, 6]. In the recent past also small systems have been considered with the advantage of a simpler secondary use of the waste heat [7,8]. The main motivation for the interest in the gas turbine and the combined cycle is its high efficiency compared to other thermal engines.

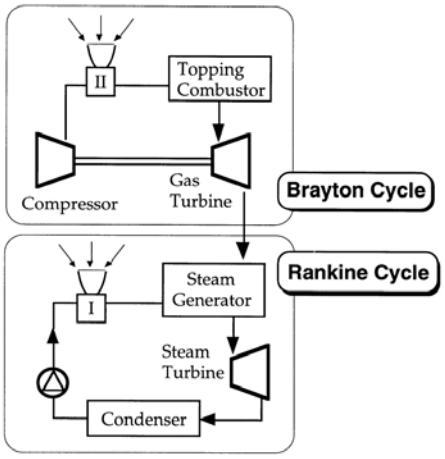

Figure 1: Options for a solar operation of a combined cycle [4]

From the options for a solar operation of a combined cycle in Figure 1, only option 2 offers high solar shares such as more than 90% or even a “solar only” operation, which would also enable to leave out the topping combustor and replace it with a thermal storage system.

The tubular receiver is a bi-functional component employed to absorb radiation (up to 1000 kW/m²) and to transfer heat to a working fluid, in case of the gas turbine it is hot pressurized air. How it principally could look like is shown in Figure 2. It also shows the main drawback of a tubular solar receiver, which is the convective thermal resistance during the heat transfer from the solid wall to the gas.

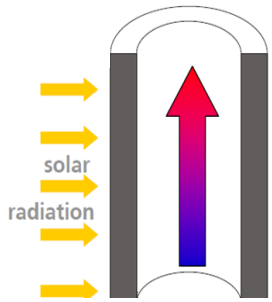

Figure 2: A tubular high temperature receiver for solar tower technology [13].

To overcome this drawback and to enable high application temperatures, a new tubular receiver has been proposed for this study, which follows a hybrid concept. The tube wall is based on a Ceramic Matrix Composite (CMC). It is connected to a ceramic porous in-lay made from reticulated foam or an engineered porous 3D-structure. By increasing the overall heat transfer surface and by minimizing the characteristic diameter representative for the flow through the open pore system of the structure the heat transfer is considered to be increased significantly. The principle concept of this approach is shown in Figure 3.

The objective of the study is to pre-qualify the material technology considered for a possible application in solar gas turbine environments.

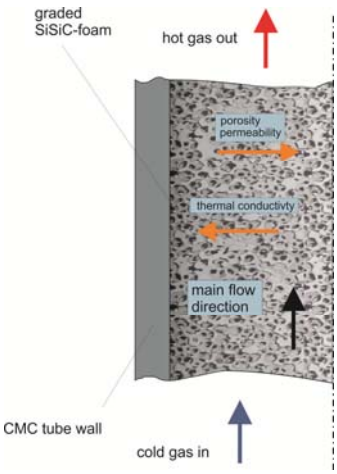

Figure 3: The concept of the present study: CMC tube wall and enhanced heat transfer with a porous in-lay

The materials investigated in this study were tubular samples consisting of tube walls, which have been manufactured from Si-infiltrated SiC fiber reinforced SiC (SiC_f/Si/SiC) and porous in-lays made out of highly cellular siliconized SiC foam (Engicer SA, Balerna, CH). Additionally and for comparison, an alternative in-lay made from a determined 3-D structure was used, which was based on a printed polymer pre-form. The processing of the samples has been already described in more detail in a prior publication [9].

2. Methodology

To predict the behaviour of the proposed material technology in real service conditions a three-stage approach has been chosen. In a first step, heat transfer and permeability characteristics have been determined experimentally at ambient pressure and temperatures below 100°. Secondly, a 2-D CFD-model has been developed for the experiment to determine the volumetric heat transfer coefficient by means of a parameter study. Finally, along with the acquired permeability coefficient this quantity was used to transfer the numerical model to high pressure and high temperature conditions.

2.1 Samples investigated and experimental set-up

From the test samples manufactured at the labs at SUPSI and Yeungnam University and delivered to DLR four have been taken for testing. Two of the "foam in-lay"- type and two of the "3D-printed in-lay" - type. The samples dimensions are 20mm in diameter and 50mm in length. The PPI-number, which denotes the number of pores along a line of one inch[1] of the foam, of the foam inlet used is slightly below 10. The tube-walls of approximately 1 mm thickness have a continuous connection to the in-lay.

A detailed description of the processing technology as well as the results of mechanical and durability testing can be found in Part 1 of the paper, which has already been published [16]. To summarize the most important properties it should be only mentioned, that for creating a dense tube wall of approximately 1mm thickness, the in-lay samples have been wrapped with 6 layers of SiC fibres yarns (Tyranno SA-3), which have been wetted before with a phenolic resin. To create a dense matrix for the tube wall, Silicon carbide and Carbon particle infiltration using Electrophoretic Deposition (EPD) has been used. Subsequently, liquid Silicon infiltration has been carried out for the reaction-bonding between Silicon and Carbon to form SiC.

[1] PPI = pores-per-inch

The mean flexural strength of the skin layer was 160,3 ± 27.6 MPa, even though it showed a brittle behaviour because the interphase layer (such as pyrolytic carbon on the SiC fibre) was not coated.

For durability testing high temperature oxidation test at 1400 & 1600C for 24 hours in air have been carried out, which have shown low oxidation rates.

Two samples of each kind have been aligned in a row to increase the overall transferred heat for more precise measurement. For comparison two additional "empty tube" samples have been investigated.

Figure 4: Test samples "foam in-lay" (left) and "3D-printed in-lay" (right) used for experimental testing

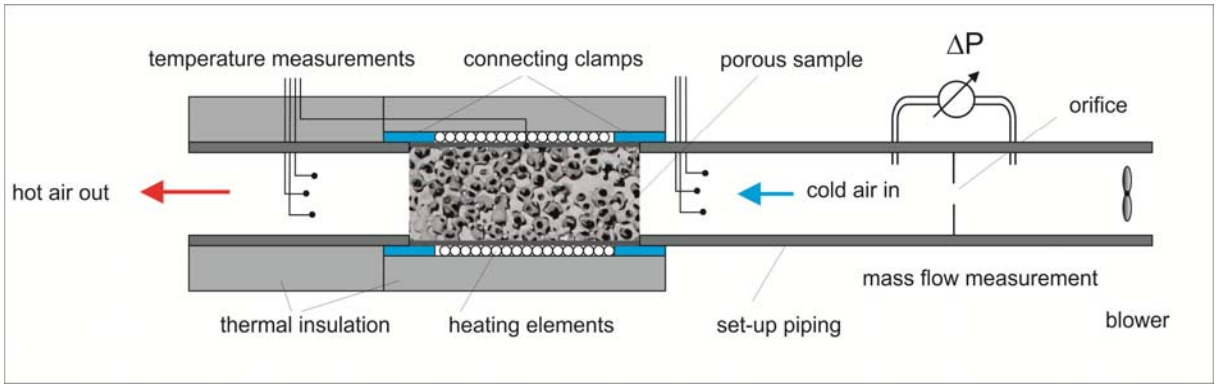

Figure 5: Experimental Set-Up for heat transfer and permeability measurement

Using VACOM[2] steel pipes KF20 with flanges and a diameter of 20mm a linear set-up schematically shown in Figure 5 has been assembled. An electrical LEISTER-Robust[3]-blower

[2] **VACOM Vakuum Komponenten & Messtechnik GmbH,** Gabelsbergerstraße 9, 07749 Jena, Germany

[3] **Leister AG,** Galileo-Straße 10, CH-6056 Kägiswil/Switzerland

was used to generate maximum air mass flows of up to 3g/s. A metering orifice along with a pressure difference measurement delivered precise mass flow data. The two aligned samples have been wrapped with a tape and enveloped with a heating wire. Temperature measurements have been performed with thermocouples to determine air in- and outlet as well as outer sample wall temperature.

For permeability measurements, the up-stream piping of the pressure difference measurement has been removed to determine the pressure drop caused by the porous sample.

2.2 Numerical Approach

The finite element solver COMSOL-Multiphysics®[4] version 3.1 has been used to develop a model describing the phenomena in the experiment and later in more realistic service conditions. The model considers the foam as well as the 3D-printed structure as a porous continuum with homogenized properties, which have been either experimentally determined (permeability), communicated from the manufacturer (tube wall thermal conductivity) or taken from structure-property-correlations of prior experimental studies. Two domains have been considered, a porous domain representing the porous in-lay and a solid domain, representing the dense tube wall. Cylindrical symmetry was assumed with the consequence, that the model could be reduced to 2 dimensions (Figure 6). In the porous domain the Brinkmann-equation for porous media describes the fluid dynamics using the measured (inertial) permeability coefficient K (column 2, line 2 in Table 1). The permeability coefficient K is one of the four effective quantities used to characterize flow and heat transport in porous media. A thorough discussion of this equation, which uses the velocity vector u and the viscosity η to describe the fluid properties and ε_p (the second effective quantity) to describe the porosity of the porous body, is provided by Ingham and Pop [15]. Furthermore, in the same porous domain, the heat transfer equations for the gaseous phase and the solid phase (column 2, line 3 and 4 of Table 19) are solved separately and simultaneously with the Brinkmann equation. This approach is known as local non thermal equilibrium (LNTE) in the literature. Thus, two temperature fields T_2 and T are calculated. Energy exchange between the gaseous phase and the solid phase is regarded by introducing a term describing the volumetric solid-to-fluid heat transfer by convection:

[4] **COMSOL AB,** Tegnérgatan 23, SE-111 40 Stockholm, Sweden

$$q_0 = \alpha \cdot A_V (T_2 - T) \qquad (1)$$

α denotes the heat transfer coefficient and A_V the specific surface area (m^2/m^3) of the cellular material. $\alpha \cdot A_V$ can be considered as the third characteristic *effective quantity* describing the capability of the cellular material to transfer heat to a gaseous medium. From the effective quantities used the volumetric heat transfer coefficient $\alpha \cdot A_V$ is the only one, which is not known exactly and which is determined by comparing experimental and numerical data. The forth effective quantity of the porous medium is its effective thermal conductivity k_{eff}. It appears in the heat transfer equation for the solid phase of the porous medium (column 2, line 4 of Table 1). It characterizes the capability of the porous medium to transport heat within the solid grid of its structure. This quantity (k_{eff} = 0,9 W/mK), which is significantly lower than the thermal conductivity of the dense material (k=85W/mK) has been taken from [12].

In the solid domain of the component, the tube wall, the numerical description of the heat transport is quite simple. Only the Fourier equation for stationary heat transport is used (column 2, line 5 of Table 1), which needs the thermal conductivity of the dense material k as a characteristic quantity for the dense tube wall.

As boundary conditions, for the fluid dynamical model, a constant fluid velocity was assumed at the inlet of the tube in contrast to constant pressure at the outlet (column 3, line 2 of Table 1). In the heat transfer equation for the gaseous phase a constant inlet gas temperature was taken as the boundary condition according to the experimental data for the calculation for the experimental case. For the “prediction at high temperatures and high pressures case”, typical gas turbine inlet temperatures of about 530°C have been assumed (column 3 line 4 of Table 1). At the outlet, “convection flow” has been assumed, which means that the gas may flow out of the component without any change in temperature any more. For the porous medium solid phase heat transfer equation it was assumed, that no heat losses occur at the in-let and out-let surfaces of the porous medium (thermal insulation). This addresses the consideration that the domain is an arbitrary sample section, which is part of a larger component. Finally, in the hat transfer equation of the solid wall, a constant outer temperature has been taken, which has been identical with the experimental data or - in the “prediction case” - with a typical solar load. For simplicity, in the latter case, a constant temperature of 1000°C was taken, which was taken as being homogeneously distributed all around the outer surface. Further information on the continuum model is contained in [10].

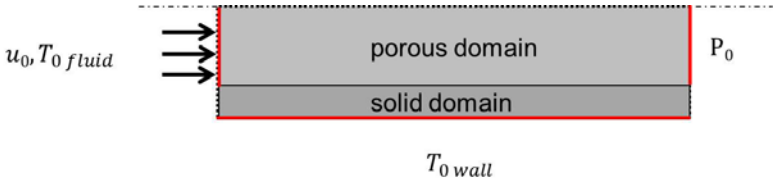

Figure 6: Reduced 2-D model of the heat-transfer tube experiment assuming cylindrical geometry

Table 1: Equations and boundary conditions used in the numerical model

Equation Description	**Domain equations**	**Boundary conditions**	
Brinkmann Equation in the *porous domain*	$\left(\frac{1}{\varepsilon_p}\right)\eta\cdot\nabla\left(\nabla u+(\nabla u)^T\right)=\left(\frac{\eta}{K}\right)\cdot u$	inlet: velocity $u=u_0$	outlet: pressure without viscous stress $p=p_0$
convection and heat conduction in the gaseous phase of the *porous domain*	$\nabla\left(-k_{fluid}\nabla T+\rho\cdot c_p\cdot u\cdot T\right)=q_0$ $q_0=\alpha\cdot A_V(T_2-T);$	inlet: temperature $T=T_{0\,fluid}$	outlet: convection flow $n\cdot\left(-k_{fluid}\cdot\nabla T\right)=0$
heat conduction in the solid phase of the *porous domain*	$-\nabla\left(k_{eff}\cdot\nabla T_2\right)=q_0$ $q_0=\alpha\cdot A_V\cdot\left(T-T_2\right)$	inlet and outlet: insulated wall	
heat conduction in the *solid domain*	$-\nabla\left(k\cdot\nabla T_2\right)=0$	$T_2=T_{0\,wall}$	

3. Results and Discussion

3.1 Experimental results

Results of permeability measurements are shown in Figure 7 as specific pressure drop versus superficial velocity plots. These plots have been fitted with second degree polynomials to derive the coefficients of the extended Darcy equation

$$\frac{\Delta p}{l} = \frac{\eta}{K_1} u - \frac{\rho}{K_2} u^2 \qquad (2)$$

according to [11]. The coefficients, $k_1 = 1{,}96 \cdot 10^{-7}$ m² and $k_2 = 3{,}53 \cdot 10^{-3}$ m for the foam and of $k_1 = -1{,}37 \cdot 10^{-5}$ m² and $k_2 = 2{,}93 \cdot 10^{-3}$ m for the printed 3d-structure, are considered to be independent of temperature and pressure and fluid properties. The experimental data are typical for foams with low PPI numbers and obviously, the 3D-printed structure shows a slightly lower permeability than the foam.

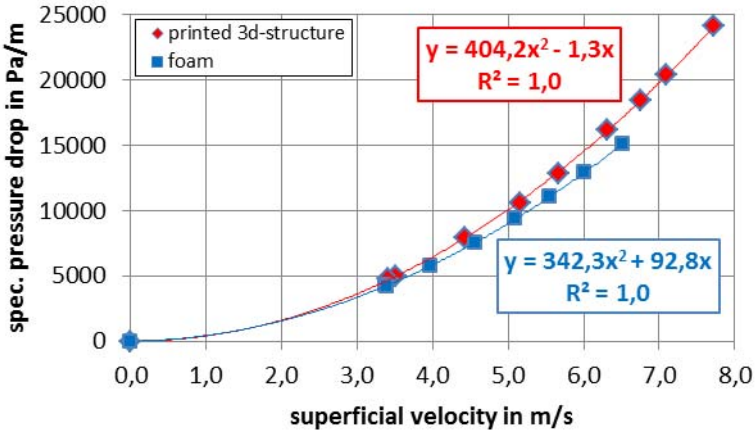

Figure 7: Results of permeability measurements

Results of heat transfer measurements are shown in Figure 8 as transferred heat (Q) versus logarithmic temperature difference plots, with $\Delta \boldsymbol{T}_{\log}$ calculated according to

$$\Delta T_{\log} = \frac{T_{out} - T_{in}}{\log[(T_W - T_{in})/(T_W - T_{out})]}. \qquad (3)$$

Foam and 3D-structure show comparable behaviour. This led us to limit our further considerations to one structure with the heat transfer properties determined. The heat transfer rate $Q/\Delta T_{\log}$ can be considered as a quantity characterizing the bulk performance of the heat

exchanger sample tested [1]. It has been determined from the slope of the curves. In Table 2, these values are listed up. The experimental determination of the empty tube case was not possible with the available set-up, because the temperature increase was too low to be precisely measured. However, tubular heat transfer can also be derived from correlations in literature. The yellow curve in Figure 8 has been calculated with a Nusselt number of 31 based on a Nusselt/Reynolds correlation for short tubes from [14]. With these data the relative performance is given, showing that the heat transfer rate of the porous case is approximately 6 times of that of the empty tube value.

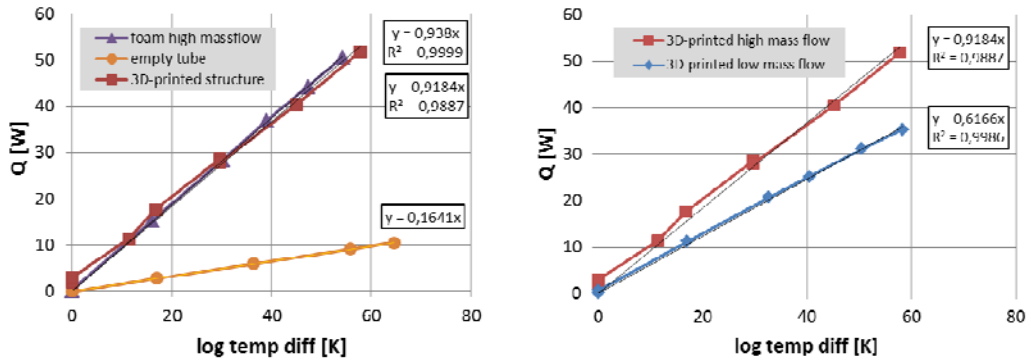

Figure 8: Results of the heat transfer measurements

For a first simple qualitative explanation of this big difference, it is useful to write the bulk heat transfer rate as

$$\frac{Q}{\Delta T_{\log}} = UA_V V \cdot \qquad (4)$$

Here, U denotes the bulk heat transfer coefficient, which refers to the difference between the outer wall temperature of the tube and the mean fluid temperature [1]. A_V denotes the specific surface area and V the volume of the whole porous domain. Whereas the specific surface area for the foam and the printed 3D structure is only about twice of the empty tube, the difference in the bulk heat transfer coefficient is much more significant. U may be derived from the dimensionless Nusselt Number (Nu) as

$$U = \frac{Nu \cdot k_{fluid}}{d_{ch}} . \qquad (5)$$

Assuming “channel flow” in both cases with comparable Nusselt numbers, a difference of a factor of approximately 3 in U may be explained with the difference in the characteristic

length, which is approximately 18 mm in case of the empty tube and 6 mm in case of the foam and the printed 3D-structure, if a ppi-number of 7 is assumed and the characteristic length is considered to be half of the pore circumference.

Table 2: Relative heat transfer performance and relevant porous media data [12]

	$Q/\Delta T_{log}$ (W/K)	relative performance -	Av (1/m)	char. Length d_{ch} (m)
empty tube	0,164	1	200	0,018
3D-printed structure	0,918	5,6	400	0,0056
foam	0,938	5,7	400	0,0056

To derive the volumetric heat transfer coefficient αA_v, which refers to the local pore-level solid-to-fluid heat transfer and consequently to the local temperature difference between the solid and the fluid phase, which is needed as a characteristic effective quantity for the porous medium to be used in eq. (1) of the numerical model, the experiment has been modelled numerically for selected fluid and temperature conditions. One example is shown in Figure 9. Here, the temperature distribution in the fluid phase as well as in the solid phase is shown along with the flow lines. The average flow velocity was approximately 6 m/s. With this model, a parameter study has been carried out to find out αA_v by variation until the calculated average air outlet temperature matched the experimental data. Finally, αA_v was determined to 27500 W/m³K for the given flow conditions. The related Nusselt Number according to eq. (5) is 6.1, which goes well with experimentally derived Nusselt numbers from 10 PPI silicon carbide foams [12].

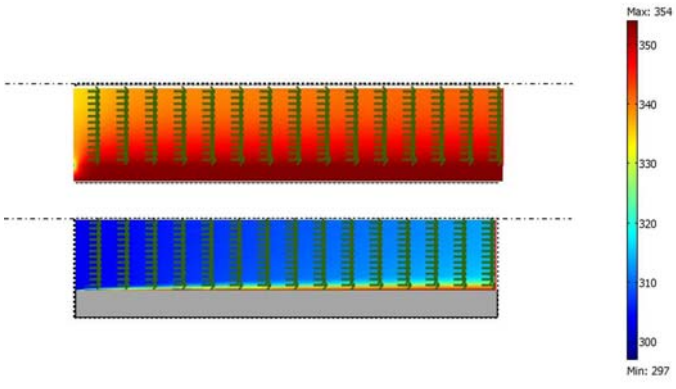

$\dot{m}$	0,002	kg/s
T_{in}	297	K
T_w	354	K
P	100000	Pa
αA_V	27500	W/m³K
λ_{eff}	3	W/mK
λ_{bulk}	48	W/mK

Figure 9: Fluid (bottom) and solid (top) temperature distribution and flow pattern according the numerical calculation and boundary/domain settings used

3.2 Performance prediction in high pressure/high temperature environments

To predict the performance of the component in gas turbine service conditions the model developed has been employed again, now using the appropriate fluid properties for higher temperatures and pressures. Permeability and Nusselt number from the “low temperature experiment” have been used. An outer wall temperature of 1273 K (1000°C), an outlet pressure of $6 \cdot 10^5$ Pa and a fluid velocity of 6 m/s were taken as boundary conditions. Figure 10 shows the corresponding gas temperature distribution inside the receiver tube for the porous case compared to the case of an empty tube. The total heat transfer amounts to 398 W compared to 115 W in case of the empty tube. In case of the porous domain, the region of heat transfer is significantly exceeding the wall region and nearly all of the porous volume participates.

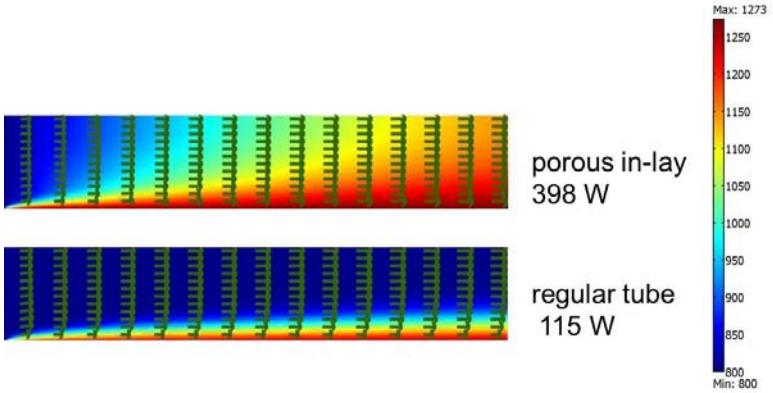

Figure 10: Fluid temperature distribution and flow pattern in the porous receiver tube compared to the empty tube case for an outer wall temperature of 1273 K and a gas pressure of 6 bars

4. Conclusions

The results show that using heat transfer enhancing geometrical features such as foams or 3D printed structures the heat transfer performance of tubes can be increased significantly. Here, the effect of the enlarged surface comes along with the decrease of the characteristic diameter representative for tubular flow. Using a numerical model describing flow and heat transfer in a porous continuum the behaviour of a tubular receiver in close-to-service-environments has been predicted. The results show, that also in high temperature and high pressure environments the overall hat transfer can be increased by approximately 4 times if a porous in-lay is used. The performance difference between the 3D-printed structure and the foam was below the uncertainty of measurement.

However, experiments in service environments and for larger flow regimes must follow to confirm the numerical predictions and to increase the reliability of the material. Additionally, more attention must be paid on a further optimization of the pore geometry of the 3D-printed structure to benefit from this new material technology.

SYMBOLS

A_V	specific surface area	[1/m]
C_p	specific heat capacity	[J/(kgK)]
d_{ch}	characteristic length	[m]
K	permeability coefficient	[m]
k_{eff}	effective thermal conductivity (porous medium)	[W/(mK)]
k	thermal conductivity (solid)	[W/(mK)]
k_{fluid}	thermal conductivity (fluid)	[W/(mK)]
K_1	viscous permeability coefficient	[m²]
K_2	inertial permeability coefficient	[m]
l	length	[m]
$\dot{m}$	mass flow rate	[kg/s]
n	normal vector	[-]
q_0	heat flow rate	[W/m²]
P	pressure	[Pa]
Q	power	[W]
T	fluid (air) temperature	[K]
T_{in}/ T_{out}	fluid temperature (in- and outlet)	[K]
T_2	solid temperature	[K]
T_w	wall temperature	[K]
u	flow velocity	[m/s]
V	volume	[m³]
α	heat transfer coefficient	[W/(m²K)]
ΔT_{log}	log. Temperature difference	[K]
ε_P	porosity	[-]
η	dynamic viscosity	[Pa s]
ρ	density	[kg/m³]

ACKNOWLEDGEMENTS

This study was supported by the KORANET (www.koranet.eu) joint call on green technologies (Grant No. NRF-2012 K1A3A7A03051754), by the Basic Science Research Program through the National Research Foundation of Korea (NRF) funded by the Ministry of Education Science and Technology (Grant No. 2012

R1A1A2000 858), by the Swiss National Science Foundation (Grant No. IZ11Z0-145220) and by the German Ministry of Education and Research (Grant No. 01DR12106).

REFERENCES

[1] F. Kreith and M. Bohn, Principles of Heat Transfer, Sixth Edition, Thomson, 2001

[2] P. Schwarzbözl, R. Buck, C. Sugarmen, A. Ring, M.J.M. Crespo, P. Altwegg, J. Enrile, Solar gas turbine systems: Design, cost and perspectives, Solar Energy 80 (2006), 1231-1240

[3] W. Grasse, H.P. Hertlein, C.-J. Winter, Thermal Solar Power Plants Experience, in: C.J. Winter, R.L. Sizmann, L.L. Vant-Hull (Eds.), Solar Power Plants, Springer, Berlin, Heidelberg, 1991, pp. 237-249.

[4] A. Kribus, R. Zaibel, D. Carey, A. Segal, J. Karnia, A solar driven combined cycle power plant, Solar Energy 62 (1998) pp. 121-129.

[5] A. Kribus, P. Doron, R. Rubin, R. Reuven, E. Taragan, S. Duchan, J. Karni, Performance of the Directly-Irradiated Annular Pressurized Receiver (DIAPR) operating at 20 Bar and 1200°C, Journal of Solar Energy Engineering, 123 (2001) pp. 10-17

[6] P. Garcia, A. Ferriere, G. Flamant, P. Costerg, R. Soler, B. Gagnepain, Solar field efficiency and electricity generation estimations for a hybrid solar gas turbine project in France, Journal of Solar Energy Engineering 130 (2008) pp. 014502.1-014502.3

[7] L. Aichmayer, J. Spelling, B. Laumert, T. Fransson, Micro Gas-Turbine Design for Small-Scale Hybrid Solar Power Plants, Journal of Engineering for Gas Turbines and Power 135 (2013) pp. 13001.1-13001.

[8] L. Aichmayer, J. Spelling, W. Wang, B. Laumert, Design and analysis of a solar receiver for micro gas turbine based solar dish systems, In: Proceedings of the 18th SolarPACES Conference, Marrakech, Morocco, 11.–14. September, 2012

[9] A. Ortona, Th. Fend, H.W. Yu, K. Raju, D.H. Yoon, Fabrication of cylindrical SiCf/Si/SiC-based composite by electrophoretic deposition and liquid silicon infiltration, Journal of the European Ceramic Society 34 (2014) pp. 1131-1138

[10] Th. Fend, P. Schwarzbözl, O. Smirnova, D. Schöllgen, C. Jakob, Numerical investigation of flow and heat transfer in a volumetric solar receiver, Renewable Energy 60 (2013) pp. 655-661

[11] M.D.M. Innocentini, P. Sepulveda, F. dos Santos Ortega, Permeability, in: M. Scheffler, P. Colombo (Eds.), Cellular Ceramics: Structure, Manufacturing, Properties and Applications, Wiley-VCH Verlag GmbH & Co. KgaA, Weinheim (2005) pp. 313-315

[12] Th. Fend, O. Reutter, D. Trimis, R. Pitz-Paal, B. Hoffschmidt, Thermal Properties, in: M. Scheffler, P. Colombo (Eds.), Cellular Ceramics: Structure, Manufacturing, Properties and Applications, Wiley-VCH Verlag GmbH & Co. KgaA, Weinheim (2005) p. 357

[13] C.K. Ho, B.D. Iverson, Review of high-temperature central receiver designs for concentrating solar power, Renewable and Sustainable Energy Reviews 29 (2014) pp. 835–846

[14] H.D. Baehr, K. Stephan, Wärme- uns Stoffübertragung, 4th. Ed., Springer, Berlin, pp. 388-390

[15] J.L. Lage, The fundamental theory of flow through permeable media from Darcy to turbulence, in: D.B. Ingham, I. Pop (Eds.), Transport phenomena in porous media, 1st. Ed., Pergamon, Oxford, 1998, pp. 14-16

[16] A. Ortona, Th. Fend, H.W. Yu, K. Raju, P. Fitriani c, D.H. Yoon, Tubular Si-infiltrated SiCf/SiC composites for solar receiver application- Part1:Fabrication by replica and electrophoretic deposition, Solar Energy Materials & Solar Cells 132(2015) pp. 123–130